13. W. R. Farmer, J. C. Liao, *Nat. Biotechnol.* **18**, 533 (2000).
14. H. Alper, K. Miyaoku, G. Stephanopoulos, *Nat. Biotechnol.* **23**, 612 (2005).
15. M. C. Chang, J. D. Keasling, *Nat. Chem. Biol.* **2**, 674 (2006).
16. V. J. Martin, D. J. Pitera, S. T. Withers, J. D. Newman, J. D. Keasling, *Nat. Biotechnol.* **21**, 796 (2003).
17. D. Morrone *et al.*, *Appl. Microbiol. Biotechnol.* **85**, 1893 (2010).
18. E. Leonard *et al.*, *Proc. Natl. Acad. Sci. U.S.A.* **107**, 13654 (2010).
19. Q. Huang, C. A. Roessner, R. Croteau, A. I. Scott, *Bioorg. Med. Chem.* **9**, 2237 (2001).
20. B. Engels, P. Dahm, S. Jennewein, *Metab. Eng.* **10**, 201 (2008).
21. L. Z. Yuan, P. E. Rouvière, R. A. Larossa, W. Suh, *Metab. Eng.* **8**, 79 (2006).
22. Y. S. Jin, G. Stephanopoulos, *Metab. Eng.* **9**, 337 (2007).
23. H. H. Wang *et al.*, *Nature* **460**, 894 (2009).
24. D. Klein-Marcuschamer, P. K. Ajikumar, G. Stephanopoulos, *Trends Biotechnol.* **25**, 417 (2007).
25. J. M. Dejong *et al.*, *Biotechnol. Bioeng.* **93**, 212 (2006).
26. Materials and methods are available as supporting material on *Science* Online.
27. K. L. Jones, S. W. Kim, J. D. Keasling, *Metab. Eng.* **2**, 328 (2000).
28. R. Kaspera, R. Croteau, *Phytochem. Rev.* **5**, 433 (2006).
29. S. Jennewein, R. M. Long, R. M. Williams, R. Croteau, *Chem. Biol.* **11**, 379 (2004).
30. M. A. Schuler, D. Werck-Reichhart, *Annu. Rev. Plant Biol.* **54**, 629 (2003).
31. E. Leonard, M. A. Koffas, *Appl. Environ. Microbiol.* **73**, 7246 (2007).
32. D. R. Nelson, *Arch. Biochem. Biophys.* **369**, 1 (1999).
33. S. Jennewein *et al.*, *Biotechnol. Bioeng.* **89**, 588 (2005).
34. D. Rontein *et al.*, *J. Biol. Chem.* **283**, 6067 (2008).
35. W. R. Farmer, J. C. Liao, *Biotechnol. Prog.* **17**, 57 (2001).
36. S. Jennewein, M. R. Wildung, M. Chau, K. Walker, R. Croteau, *Proc. Natl. Acad. Sci. U.S.A.* **101**, 9149 (2004).
37. K. Walker, R. Croteau, *Phytochemistry* **58**, 1 (2001).
38. We thank R. Renu for extraction, purification, and characterization of metabolite Indole; C. Santos for providing the pACYCmelA plasmid, constructive suggestions during the experiments, and preparation of the manuscript; D. Dugar, H. Zhou, and X. Huang for helping with experiments and suggestions; and K. Hiller for data analysis and comments on the manuscript. We gratefully acknowledge support by the Singapore-MIT Alliance (SMA-2) and NIH, grant 1-R01-GM085323-01A1. B.P. acknowledges the Milheim Foundation Grant for Cancer Research 2006-17. A patent application that is based on the results presented here has been filed by MIT. P.K.A. designed the experiments and performed the engineering and screening of the strains; W-H.X. performed screening of the strains, bioreactor experiments, and GC-MS analysis; F.S. carried out the quantitative PCR measurements; O.M. performed the extraction and characterization of taxadiene standard; E.L., Y.W., and B.P. supported with cloning experiments; P.K.A., K.E.J.T., T.H.P., B.P. and G.S. analyzed the data; P.K.A., K.E.J.T., and G.S. wrote the manuscript; G.S. supervised the research; and all of the authors contributed to discussion of the research and edited and commented on the manuscript.

Supporting Online Material

www.sciencemag.org/cgi/content/full/330/6000/70/DC1
Materials and Methods
SOM Text
Figs. S1 to S11
Tables S1 to S4
References

29 April 2010; accepted 9 August 2010
10.1126/science.1191652

Reactivity of the Gold/Water Interface During Selective Oxidation Catalysis

Bhushan N. Zope, David D. Hibbitts, Matthew Neurock, Robert J. Davis*

The selective oxidation of alcohols in aqueous phase over supported metal catalysts is facilitated by high-pH conditions. We have studied the mechanism of ethanol and glycerol oxidation to acids over various supported gold and platinum catalysts. Labeling experiments with $^{18}O_2$ and $H_2{}^{18}O$ demonstrate that oxygen atoms originating from hydroxide ions instead of molecular oxygen are incorporated into the alcohol during the oxidation reaction. Density functional theory calculations suggest that the reaction path involves both solution-mediated and metal-catalyzed elementary steps. Molecular oxygen is proposed to participate in the catalytic cycle not by dissociation to atomic oxygen but by regenerating hydroxide ions formed via the catalytic decomposition of a peroxide intermediate.

The selective oxidation of alcohols with molecular oxygen over gold (Au) catalysts in liquid water offers a sustainable, environmentally benign alternative to traditional processes that use expensive inorganic oxidants and harmful organic solvents (*1*, *2*). These catalytic transformations are important to the rapidly developing industry based on the conversion of biorenewable feedstocks to higher-valued chemicals (*3*, *4*) as well as the current production of petrochemicals. Although gold is the noblest of metals (*5*), the water/Au interface provides a reaction environment that enhances its catalytic performance. We provide here direct evidence for the predominant reaction path during alcohol oxidation at high pH that includes the coupling of both solution-mediated and metal-catalyzed elementary steps.

Alcohol oxidation catalyzed by Pt-group metals has been studied extensively, although the precise reaction path and extent of O_2 contribution are still under debate (*4*, *6*–*8*). The mechanism for the selective oxidation of alcohols in liquid water over the Au catalysts remains largely unknown (*6*, *9*), despite a few recent studies with organic solvents (*10*–*12*). In general, supported Au nanoparticles are exceptionally good catalysts for the aerobic oxidation of diverse reagents ranging from simple molecules such as CO and H_2 (*13*) to more complex substrates such as hydrocarbons and alcohols (*14*). Au catalysts are also substrate-specific, highly selective, stable against metal leaching, and resistant to overoxidation by O_2 (*6*, *15*, *16*). The active catalytic species has been suggested to be anionic Au species (*17*), cationic Au species (*18*, *19*), and neutral Au metal particles (*20*). Moreover, the size and structure of Au nanoparticles (*21*, *22*) as well as the interface of these particles with the support (*23*) have also been claimed to be important for catalytic activity. For the well-studied CO oxidation reaction, the presence of water vapor increases the observed rate of the reaction (*24*–*26*). Large metallic Au particles and Au metal powder, which are usually considered to be catalytically inert, have considerable oxidation activity under aqueous conditions at high pH (*27*, *28*). We provide insights into the active intermediates and the mechanism for alcohol oxidation in aqueous media derived from experimental kinetic studies on the oxidation of glycerol and ethanol with isotopically labeled O_2 and H_2O over supported Au and Pt catalysts, as well as ab initio density functional theory calculations on ethanol oxidation over metal surfaces.

Previous studies indicate that alcohol oxidation over supported metal catalysts (Au, Pt, and Pd) proceeds by dehydrogenation to an aldehyde or ketone intermediate, followed by oxidation to the acid product (Eq. 1)

$$RCH_2OH \xrightarrow{O_2,\text{catalyst}} RCH{=}O \xrightarrow{O_2,\text{catalyst}} RCOOH \quad (1)$$

Hydroxide ions play an important role during oxidation; the product distribution depends on pH, and little or no activity is seen over Au catalysts without added base. We studied Au particles of various sizes (average diameter ranging from 3.5 to 10 nm) on different supports (TiO_2 and C) as catalysts for alcohol oxidation and compared them to Pt and Pd particles supported on C. The oxidation of glycerol ($HOCH_2CHOHCH_2OH$) to glyceric ($HOCH_2CHOHCOOH$) and glycolic ($HOCH_2COOH$) acids occurred at a turnover frequency (TOF) of 6.1 and 4.9 s^{-1} on Au/C and Au/TiO_2, respectively, at high pH (>13) whereas the TOF on supported Pt and Pd (1.6 and 2.2 s^{-1}, respectively) was slightly lower at otherwise identical conditions (Table 1). For these Au catalysts, particle size and support composition had negligible effect on the rate or selectivity. In the absence of base, the glycerol oxidation rate was much lower over the Pt and Pd catalysts and no conversion was observed over the Au catalysts (Table 1). Moreover, the products detected over Pt and Pd in the absence of base are primarily the intermediate aldehyde and ketone, rather than acids.

Department of Chemical Engineering, University of Virginia, 102 Engineers' Way, Post Office Box 400741, Charlottesville, VA, 22904–4741, USA.

*To whom correspondence should be addressed. E-mail: rjd4f@virginia.edu

The effect of initial base concentration on the activity of glycerol oxidation on the supported Pt catalyst was further studied by varying the initial NaOH concentration from 0 to 0.6 M. The TOF for glycerol oxidation over Pt was proportional to the initial hydroxide concentration and thus the initial glycerolate concentration formed by the deprotonation of glycerol [Table 1, fig. S1, and supporting online material (SOM) text], which is consistent with prior work with a supported Au catalyst (*29*). Although the turnover frequencies for ethanol (CH_3CH_2OH) oxidation to acetic acid (CH_3COOH) over the above-mentioned Au and Pt catalysts were an order of magnitude lower than those observed for glycerol oxidation at identical conditions, Au was still more active than Pt for ethanol oxidation at high pH (table S1).

In an aqueous environment, the initial deprotonation of the alcohol to form an alkoxy intermediate occurs in basic solution, and the extent of the reaction is related to the system pH [the pK_a (where K_a is the acid dissociation constant) of alcohols is approximately 16] (*30*). The initial activation of the alcohol can also occur on the catalyst surface. The calculated activation barriers for the dissociative adsorption of ethanol (Fig. 1A) over the Au(111) and Pt(111) surfaces in liquid water are calculated to be very high at 204 and 116 kJ mol^{-1}, and thus O-H bond activation by the metal alone is unlikely. The presence of surface-bound hydroxide intermediates, however, can facilitate O-H bond activation via proton transfer in much the same way as it occurs in solution. This process lowers the activation barrier to less than 25 kJ mol^{-1} for either metal (Fig. 1B). The presence of adsorbed hydroxide intermediates also lowers the barrier for the subsequent activation of the C-H bond of the ensuing alkoxide intermediate to form the aldehyde over Au. (For Pt, this step already has a very low barrier over the metal without the assistance of adsorbed OH.) The ability of adsorbed hydroxide to activate both the C-H and O-H bonds so effectively on Au(111) helps to explain the overall increase in catalytic activity of the noble metal at high pH.

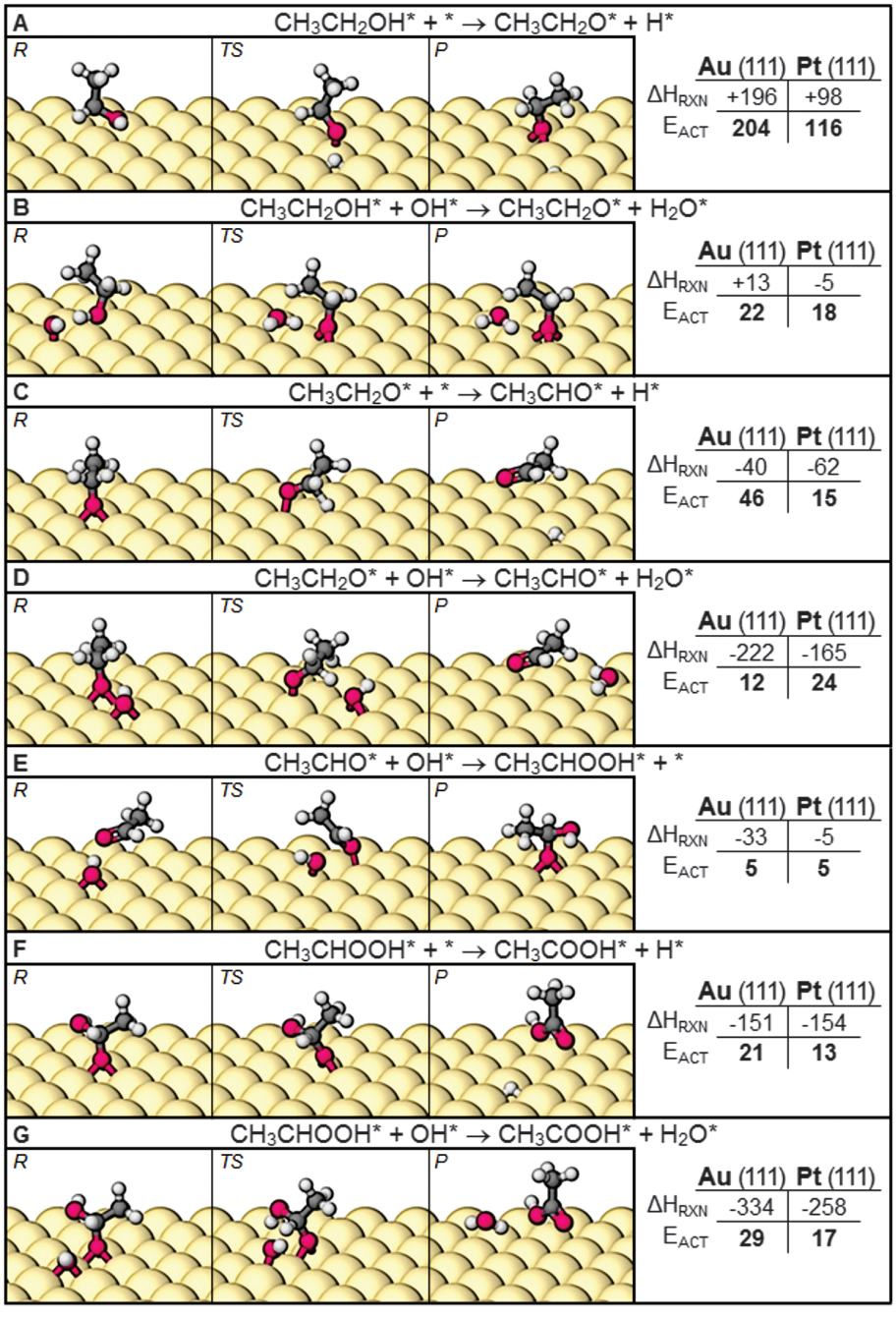

Fig. 1. (**A** to **G**) Selected reaction energies and activation barriers (in kilojoules per mole) for the oxidation of ethanol to acetic acid on Au(111) and Pt(111) surfaces in the presence of liquid water. The reactant (R), transition state (TS), and product (P) on the surfaces were computed with density functional theory. The solution-phase water was omitted for clarity.

It is unclear whether O atoms derived from O_2 or from hydroxide ions are involved in carboxylate formation from the intermediate aldehyde. To determine the role of O_2 in the mechanism, the oxidation of aqueous-phase glycerol and ethanol was performed in a batch autoclave reactor using $^{18}O_2$ in the presence of base (0.3 M glycerol or ethanol and 0.6 M NaOH) together with either Au/C or Au/TiO_2 (0.8 and 1.6% Au, respectively, obtained from the World Gold Council) as a catalyst (*31*). The isotopomer distribution in the product was evaluated by mass spectrometry. Glyceric acid was the major product of glycerol oxidation for all catalysts evaluated at high pH (Table 1). However, no discernable amount of labeled O was observed in the glyceric acid product. Figure 2 shows a representative reaction profile for the oxidation of glycerol as well as the mass spectrum of the product glyceric acid. For the reaction performed with $^{18}O_2$, only one peak in the mass spectrum of glyceric acid corresponding to the unlabeled product was observed (fig. S2). Analogous experiments with ethanol oxidation confirmed a lack of ^{18}O incorporation into the product acetic acid (fig. S5). Regardless of the Au particle size, the composition of the support, and the structure of the alcohol, ^{18}O was not observed in the products of alcohol oxidation.

The lack of ^{18}O incorporation in the acid products might be caused by an inability of Au nanoparticles to dissociatively adsorb O_2 (*14*, *32*, *33*). We studied glycerol oxidation over C-supported Pt (1%, obtained from Sigma-Aldrich) and Pd (3%, Sigma-Aldrich) with $^{18}O_2$ at high pH (*31*), because these transition metals dissociate O_2 (*34*). However, no labeled O was observed in the glyceric acid product (fig. S2, B and C). Because base is not required to oxidize alcohols over Pt, glycerol oxidation was carried out with $^{18}O_2$ over Pt/C in neutral water. Again, no ^{18}O-labeled acid products were observed in any appreciable amounts (fig. S2D), which is con-

sistent with prior work involving ethanol oxidation over Pt in neutral solution (*35*). To confirm that the acid products do not exchange O appreciably with liquid water, the major products from glycerol and ethanol oxidation (glyceric, glycolic, and acetic acid) were dissolved separately in $H_2{}^{18}O$ and heated to the reaction conditions in the presence of base and a Au catalyst for the duration of a typical reaction test (3 hours). No appreciable incorporation of ^{18}O from labeled water was observed in the products (figs. S2 to S5). It should be emphasized that no glycerol oxidation was observed in the absence of O_2.

To explore the role of hydroxide in Au-catalyzed oxidation, glycerol and ethanol were oxidized over Au/C and Au/TiO_2 with labeled water ($H_2{}^{18}O$) at high pH (0.3 M glycerol or ethanol and 0.6 M NaOH) and $^{16}O_2$ as the gas-phase oxidant. The mass spectrum for glyceric acid produced during glycerol oxidation (Fig. 2 and fig. S2) shows that a range from one to four ^{18}O atoms was incorporated into the glyceric acid product. Incorporation of multiple labeled ^{18}O atoms into the acetic acid product of ethanol oxidation over Au/C and Au/TiO_2 (fig. S5) and into the minor oxidation products of glycerol was also observed (figs. S3 and S4). Because the reaction products do not exchange O with water on the time scale of the reaction, the appearance of ^{18}O in the product during reactions performed in $H_2{}^{18}O$ suggests that aqueous-phase alcohol oxidation proceeds through an alkoxy intermediate of the geminal diol that was formed by the reaction of the aldehyde intermediate with hydroxide (Figs. 1E and 3). Rapid exchange of the diols with $^{18}OH^-$ accounts for the two ^{18}O atoms found in the acetic acid product from ethanol oxidation. During glycerol oxidation, glyceraldehyde ($HOCH_2CHOHCHO$) is the reaction intermediate produced by the initial dehydrogenation of the terminal alcohol of glycerol. The base-catalyzed rapid interconversion of glyceraldehyde to dihydroxyacetone ($HOCH_2COCH_2OH$) (DHA) during the oxidation reaction could account for more than two ^{18}O atoms appearing in the product (SOM text) (*36*). Indeed, a control experiment with glyceraldehyde (0.05 M) in the presence of Au/C and a small amount of base (0.01 M NaOH to avoid degradation of glyceraldehyde) in $H_2{}^{18}O$ resulted in ^{18}O incorporation in DHA that was formed during the experiment, as seen in fig. S6.

Theory was used to examine the base-catalyzed aqueous-phase oxidation of acetaldehyde (CH_3CHO) in solution, as shown in Eq. 2, and to explore the role of hydroxide ion as the oxygen source

$$CH_3CHO + HO^- \rightarrow CH_3CHOOH^- \quad (2)$$

The activation barrier for this reaction in solution was calculated to be 45 kJ mol^{-1}. The barrier is largely due to the energy required to restructure the H-bonding water network around the solvated hydroxide anion and the aldehyde to allow them to react together. The same reaction was also examined on the Au(111) and Pt(111) surfaces in the presence of solvent, which resulted in activation barriers of 5 kJ mol^{-1} for both metals (Fig. 1E).

Table 1. Glycerol oxidation over Au/C, Au/TiO_2, Pt/C, and Pd/C in liquid water.

Catalyst	NaOH: glycerol (mol:mol)	TOF (s^{-1})	Conversion (%)	Selectivity (%)				
				Glyceric acid	Glycolic acid	Tartronic acid	Glyceraldehyde	Dihydroxy-acetone
Au/C*	2.0	6.1	6.8	67	33	0.0	0.0	0.0
Au/TiO_2*	2.0	4.9	33	64	24	2.0	0.0	0.0
Pd/C*	2.0	2.2	29	83	6.0	5.0	0.0	0.0
Pt/C*	2.0	1.6	16	70	21	7.0	0.0	0.0
Pt/C*	1.0	0.76	7.1	78	14	7.0	0.0	0.0
Pt/C*	0.5	0.48	4.7	72	28	0.0	0.0	0.0
Pt/C†	3×10^{-4}	0.05	8.0	29	0.0	0.0	50	21
Pt/C†	0.0	0.06	9.0	25	0.0	0.0	54	21
Pd/C†	0.0	0.004	1.3	25	0.0	0.0	50	25
Au/C†	0.0	0.0	0.0	0.0	0.0	0.0	0.0	0.0
Au/TiO_2†	0.0	0.0	0.0	0.0	0.0	0.0	0.0	0.0

*Reaction conditions: 0.3 M glycerol (*G*); 30 ml; at 333 K; PO_2 = 11 bar; G:Au = G:Pt = 8000 (mol:mol); G:Pd = 2500 (mol:mol); time (*t*) = 0.5 hours. †Reaction conditions: 0.3 M glycerol; 5 ml; at 333 K; PO_2 = 11 bar; G:Au = G:Pt = 5000 (mol:mol); G:Pd = 2000 (mol:mol); *t* = 5 hours. Gold particle sizes: Au/C = 10.5 nm, Au/TiO_2 = 3.5 nm. Dispersion (estimated ratio of surface to total metal atoms): Au/C = 0.05, Au/TiO_2 = 0.29, Pt/C = 0.43, Pd/C = 0.33 (*31*).

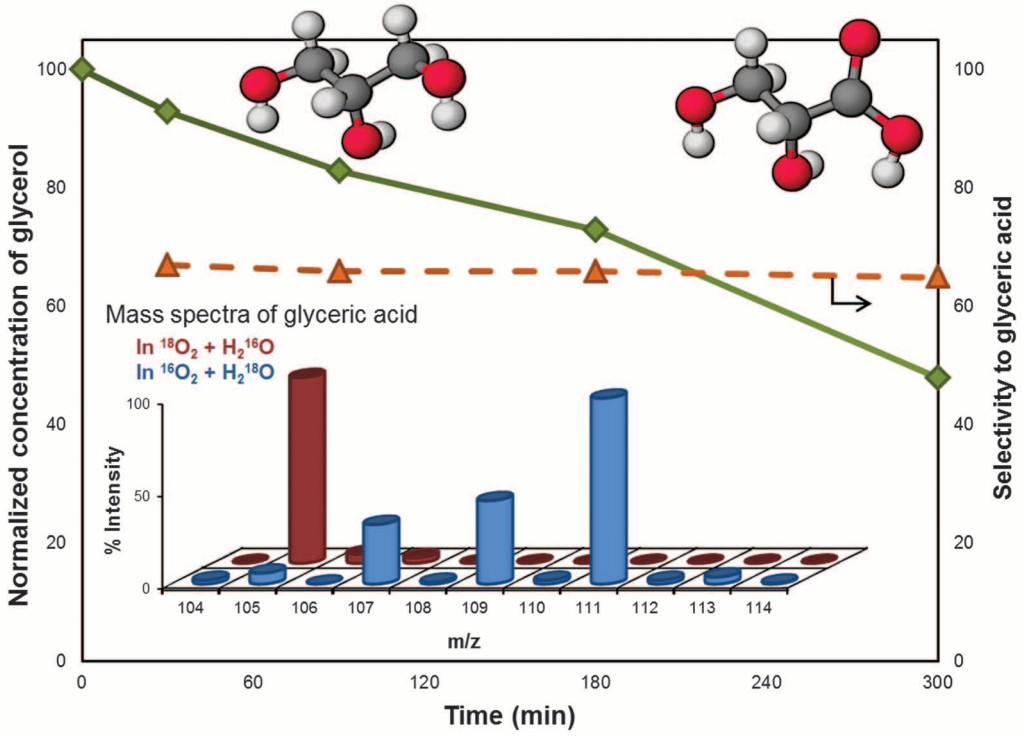

Fig. 2. Reaction profile for the oxidation of glycerol over Au/C in liquid water. Reaction conditions were as follows: 0.3 M glycerol; NaOH: glycerol = 2.0 (mol:mol); glycerol: Au = 8000:1 (mol:mol); at a temperature of 333 K; with a partial pressure of O_2 (PO_2) = 11 bar. (Inset at bottom) LC mass spectrum (electronegative ion mode) of glyceric acid (molecular weight 106) formed during glycerol oxidation over Au/C in $^{18}O_2 + H_2{}^{16}O$ or $^{16}O_2 + H_2{}^{18}O$. Glycerol oxidation in $^{16}O_2 + H_2{}^{18}O$ results in the incorporation of multiple ^{18}O atoms in the product glyceric acid. *m/z*, mass/charge ratio.

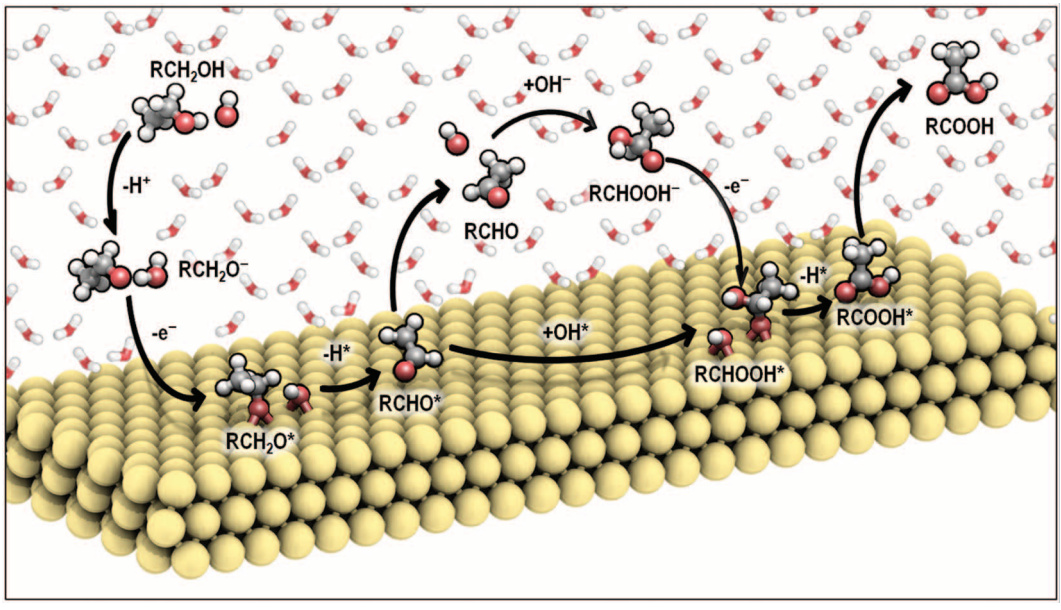

Fig. 3. Reaction scheme for the oxidation of alcohols to acids over a Au surface in water at high pH. Hydroxide facilitates elementary steps in alcohol oxidation in both the solution phase and at the metal/solution interface.

These results account for the increase in reactivity with HO^- either in solution or at the solution/metal interface. The subsequent C-H activation of the CH_3CHOOH^- intermediate to form acetic acid occurs quite readily over Pt as well as Au, with barriers of only 10 to 20 kJ mol^{-1} (Fig. 1F).

Several roles for O_2 during the oxidation reactions in water at high pH have been proposed, including the direct participation of atomic O during dehydrogenation reactions, the reduction of atomic O to water through H atoms adsorbed on the surface, the direct oxidation of the intermediate aldehyde with atomic O to form the O-insertion product acids, and the removal of strongly bound organic adsorbates such as CO through oxidation (*6*). All of these routes require O_2 dissociation on the catalyst surface, which is not favored on Au catalysts (*14*, *32*, *33*) and may be inhibited by water or hydroxides that adsorb on Pt-group catalysts. The activation barriers for O_2 dissociation on Au(111) and Pt(111) were calculated to be 105 and 64 kJ mol^{-1}, respectively, confirming the noble nature of Au as compared to Pt-group metals (table S3, reaction 7).

The production of peroxide during oxidation reactions over Au (*28*, *29*) indicates that O_2 is first reduced during these reactions before dissociation. [For the case of Pt, O_2 dissociation is also difficult because of the high surface coverages of hydroxide intermediates (*8*).] Activation of O_2 occurs through the formation and dissociation of peroxide (OOH*) and hydrogen peroxide (HOOH*) intermediates (Eqs. 3 to 5) analogous to those formed electrocatalytically under alkaline conditions via four-electron or two-electron processes (*37*)

$$O_2^* + H_2O^* \rightarrow OOH^* + HO^* \quad (3)$$

$$OOH^* + H_2O^* \rightarrow H_2O_2^* + HO^* \quad (4)$$

$$HO^* + e^- \leftrightarrow HO^- + * \quad (5)$$

where * represents a site on the metal surface. This sequence accounts for the removal of electrons added to the surface during the adsorption of hydroxide ions and the regeneration of HO^- species via O_2 reduction with water, thus closing the catalytic cycle. The steady-state coverage of hydroxide on the surface is probably limited by the ability of the metal to accommodate the excess negative charge.

To test the feasibility of this reduction sequence, density functional theory calculations were carried out over both Au and Pt surfaces. Reduction of O_2 by water had a low barrier of 16 kJ mol^{-1} on Au(111). The peroxide that forms can subsequently dissociate on Au to form atomic O and hydroxide, with a barrier of 83 kJ mol^{-1}; however, the more likely step is the further reduction of OOH* to H_2O_2*, with a barrier of only 48 kJ mol^{-1} (table S3). The decomposition of H_2O_2* to hydroxide has an activation barrier of 71 kJ mol^{-1}. The decomposition of hydrogen peroxide over Pt and Pd has a barrier of only 29 and 5 kJ mol^{-1}, respectively. The low calculated barrier for peroxide decomposition on Pd as compared to Au explains why Ketchie *et al*. observed appreciable concentrations of peroxide in the product mixture formed during glycerol oxidation over Au/C, whereas only trace amounts of peroxide were detected when Pd/C was used as a catalyst at identical reaction conditions (*38*). Our computational results, coupled with the isotopic labeling studies, demonstrate that the role of O_2 during alcohol oxidation is an indirect one that does not involve incorporation into the acid products but instead regenerates hydroxide ions.

References and Notes

1. R. A. Sheldon, J. Dakka, *Catal. Today* **19**, 215 (1994).
2. A. Corma, H. Garcia, *Chem. Soc. Rev.* **37**, 2096 (2008).
3. P. Gallezot, *Catal. Today* **37**, 405 (1997).
4. M. Besson, P. Gallezot, *Catal. Today* **57**, 127 (2000).
5. B. Hammer, J. K. Norskov, *Nature* **376**, 238 (1995).
6. T. Mallat, A. Baiker, *Chem. Rev.* **104**, 3037 (2004).
7. J. A. A. Van den Tillaart, B. F. M. Kuster, G. B. Marin, *Appl. Catal. A* **120**, 127 (1994).
8. V. R. Gangwal, J. van der Schaaf, B. F. M. Kuster, J. C. Schouten, *J. Catal.* **229**, 389 (2005).
9. G. C. Bond, D. T. Thompson, *Gold Bull.* **33**, 41 (2000).
10. A. Abad, A. Corma, H. García, *Chemistry* **14**, 212 (2008).
11. P. Fristrup, L. B. Johansen, C. H. Christensen, *Catal. Lett.* **120**, 184 (2008).
12. M. Conte, H. Miyamura, S. Kobayashi, V. Chechik, *J. Am. Chem. Soc.* **131**, 7189 (2009).
13. M. Haruta, N. Yamada, S. Iijima, T. Kobayashi, *J. Catal.* **115**, 301 (1989).
14. G. C. Bond, C. Louis, D. T. Thompson, *Catalysis by Gold*, vol. 6 of *Catalytic Science Series* (Imperial, London, 2006).
15. S. Carrettin, P. McMorn, P. Johnston, K. Griffin, G. J. Hutchings, *Chem. Commun.* **7**, 696 (2002).
16. L. Prati, M. Rossi, *J. Catal.* **176**, 552 (1998).
17. A. Sanchez *et al*., *J. Phys. Chem. A* **103**, 9573 (1999).
18. Q. Fu, H. Saltsburg, M. Flytzani-Stephanopoulos, *Science* **301**, 935 (2003).
19. J. Guzman, B. C. Gates, *J. Am. Chem. Soc.* **126**, 2672 (2004).
20. M. Haruta, M. Daté, *Appl. Catal. A* **222**, 427 (2001).
21. M. Valden, X. Lai, D. W. Goodman, *Science* **281**, 1647 (1998).
22. N. Lopez, J. K. Nørskov, *J. Am. Chem. Soc.* **124**, 11262 (2002).
23. M. Haruta *et al*., *J. Catal.* **144**, 175 (1993).
24. R. A. Ojifinni *et al*., *J. Am. Chem. Soc.* **130**, 6801 (2008).
25. M. C. Kung, R. J. Davis, H. H. Kung, *J. Phys. Chem. C* **111**, 11767 (2007).
26. M. Daté, M. Okumura, S. Tsubota, M. Haruta, *Angew. Chem. Int. Ed.* **43**, 2129 (2004).
27. W. C. Ketchie, Y. Fang, M. S. Wong, M. Murayama, R. J. Davis, *J. Catal.* **250**, 94 (2007).
28. M. A. Sanchez-Castillo, C. Couto, W. B. Kim, J. A. Dumesic, *Angew. Chem. Int. Ed.* **43**, 1140 (2004).
29. W. C. Ketchie, M. Murayama, R. J. Davis, *Top. Catal.* **44**, 307 (2007).
30. P. Ballinger, F. A. Long, *J. Am. Chem. Soc.* **82**, 795 (1960).
31. Materials and methods are available as supporting material on *Science* Online.
32. T. V. W. Janssens *et al*., *Top. Catal.* **44**, 15 (2007).

33. X. Deng, B. K. Min, A. Guloy, C. M. Friend, *J. Am. Chem. Soc.* **127**, 9267 (2005).
34. P. D. Nolan, B. R. Lutz, P. L. Tanaka, J. E. Davis, C. B. Mullins, *J. Chem. Phys.* **111**, 3696 (1999).
35. M. Rottenburg, P. Baertschi, *Helv. Chim. Acta* **227**, 1073 (1956).
36. J. Clayden, N. Greeves, S. Warren, P. Wothers, *Organic Chemistry* (Oxford Univ. Press, New York, 2000).
37. A. A. Gewirth, M. S. Thorum, *Inorg. Chem.* **49**, 3557 (2010).
38. W. C. Ketchie, M. Murayama, R. J. Davis, *J. Catal.* **250**, 264 (2007).

39. This work was supported by grants from NSF (CTS-0624608, OISE 0730277, and EEC-0813570) and the U.S. Department of Energy (DOE) (Basic Energy Sciences DE-FG02-03ER15460). We also kindly acknowledge the supercomputing time at the Environmental Molecular Science Laboratory, a national scientific user facility sponsored by the DOE's Office of Biological and Environmental Research located at Pacific Northwest National Laboratory, and the National Center for Computational Sciences at Oak Ridge National Laboratory.

Supporting Online Material
www.sciencemag.org/cgi/content/full/330/6000/74/DC1
Materials and Methods
SOM Text
Figs. S1 to S8
Scheme S1
Tables S1 to S4
References

13 July 2010; accepted 30 August 2010
10.1126/science.1195055

Human Adaptation and Plant Use in Highland New Guinea 49,000 to 44,000 Years Ago

Glenn R. Summerhayes,[1]* Matthew Leavesley,[2] Andrew Fairbairn,[3] Herman Mandui,[4] Judith Field,[5] Anne Ford,[1] Richard Fullagar[6]

After their emergence by 200,000 years before the present in Africa, modern humans colonized the globe, reaching Australia and New Guinea by 40,000 to 50,000 years ago. Understanding how humans lived and adapted to the range of environments in these areas has been difficult because well-preserved settlements are scarce. Data from the New Guinea Highlands (at an elevation of ~2000 meters) demonstrate the exploitation of the endemic nut *Pandanus* and yams in archaeological sites dated to 49,000 to 36,000 years ago, which are among the oldest human sites in this region. The sites also contain stone tools thought to be used to remove trees, which suggests that the early inhabitants cleared forest patches to promote the growth of useful plants.

Sahul, the single Pleistocene continent linking New Guinea, Australia, and Tasmania, is thought to have been colonized by humans some time after 50,000 years ago (*1*). Reaching Sahul required crossing water from Southeast Asia. Most early sites in New Guinea have been found along the coastal margins (Fig. 1, inset; fig S1; and table S2). An exception first documented in the 1960s is an open site [Papua New Guinea (PNG) National Museum site code AER] in the Ivane Valley of the New Guinea Highlands, where excavations at the Kosipe Mission recovered stone artefacts including waisted tools dated then to 26,870 ± 590 ^{14}C years before the present (radiocarbon lab no. ANU-191) (calibrated to 30,350 to 32,580 years ago) (*2*). Kosipe Mission is located at ~2000 m above sea level, on the spur of a hill overlooking a large swamp (Fig. 1). Further excavations in 2005 (*3*) extended known occupation there to 41,000 to 38,000 years ago (table S1). A carbonized kernel of a pandanus nut was recovered in the 36,000- to 34,000-year-old levels.

Subsequent fieldwork in 2007 and 2008 has identified late Pleistocene to Holocene occupation at seven additional locations across the Ivane Valley, with the earliest site dating to between 49,000 and 43,000 calibrated years before the present (table S1). Here we describe the evidence for early occupation of these sites and the subsistence strategies employed by these early colonists.

Sediments in the Ivane valley are dominated by a series of volcanic tephras that are probably derived from Mount Lamington some 140 km to the southeast. All eight highland sites have a basic set of five identified layers: a dark brown topsoil (layer 1), a brown-orange clay (layer 2); a black-brown soil (layers 3a and 3b), and a gray soil (layer 4). These occupation layers overlay culturally sterile orange clay (layer 5). Layer 3 is separated into two distinct units (a and b) at Vilakuav (*2*), representing separate ash falls. We subsequently identified these two layers (3a and 3b) in most sites. At Vilakuav, Joe's Garden, and Kosipe Mission, they are separated by a thin band of charcoal (fig. S2). Accelerator mass spectrometry dates were derived from charcoal collected in situ. We use the calibrated dates (*4*) in our discussion. All dates from Joe's Garden, Vilakuav, South Kov, and Airport Mound are presented here for the first time.

The earliest dates for occupation of the valley are at Vilakuav, between 49,000 and 43,000 years ago; and three sites (Vilakuav, South Kov, and Airport Mound) contain artefacts that yield calibrated ^{14}C dates earlier than 42,500 years ago, at 95.4% confidence levels. Occupation at the Kosipe Mission site is dated to 41,400 to 38,000 years ago, again at a 95.4% confidence level. Layer 3b shows occupation from 38,500 to 30,000 years ago, and layer 3a dates from 30,000 to 26,000 years ago. Layer 2 dates to the Holocene (table S1).

Our radiocarbon ages are some of the oldest dates for any Sahul site (table S2), excluding several contentious 20-year-old claims in Australia (*1*). Together with indirectly dated artefacts from Bobongara on the Huon Peninsula, the oldest occupational layers at the highland sites of Vilakuav, Airport Mound, and South Kov are older than any other known sites in New Guinea or Island Melanesia.

All highland sites lack evidence of any occupation during the Last Glacial Maximum (LGM). The mean temperature of the coldest month at Kosipe at the LGM has been estimated to have been between 6.3° to 9.2°C colder than today (*5*, *6*). The climates before the LGM would also have been cooler than those today. Layers 4 and 3b from the Ivane Valley correspond to marine isotope stage (MIS) 3, whereas layer 3a corresponds with the shift to much colder conditions from MIS 3 to MIS 2 (*7*). Other palynological evidence from the Ivane Valley (*6*) also indicates that the tree line was lower during the deposition of layers 4 and 3 and that the vegetation zones were compressed downward during the earliest occupation, which is consistent with a colder climate.

Stone artefacts were recovered from the earliest levels (layer 4) of Kosipe Mission, Airstrip Mound, South Kov, and Vilakuav (Fig. 2). Artefacts are made from a diverse range of raw materials, including basalt, schist, baked siliceous metasediment, dolerite, metabasalt, and quartz. Of these, baked siliceous sediment is the only rock type not found in the Ivane Valley. Samples of this rock were obtained along the Kosipe-Woitape track above Woitape, ~20 km distant. It is valuable for making tools because it flakes easily yet is hard.

Two waisted stone artefacts made from schist and metabasalt were found from layer 4 at South Kov and one from layer 4 at Airstrip Mound (Fig. 2 and fig. S3). This distinctive ar-

[1]Department of Anthropology, Gender and Sociology, University of Otago, Post Office Box 56, Dunedin, New Zealand. [2]Department of Anthropology, University of Papua New Guinea, Post Office Box 320, University Post Office, National Capital District, Papua New Guinea. [3]Department of Archaeology, School of Social Science, University of Queensland, Brisbane, Queeensland 4072, Australia. [4]National Museum and Art Gallery of Papua New Guinea, Post Office Box 5560, Boroko National Capital District, Papua New Guinea. [5]Australian Centre for Microscopy and Microanalysis F09, University of Sydney, New South Wales 2006, Australia. [6]Scarp Archaeology, Post Office Box 7241, South Sydney Hub, New South Wales 2015, Australia.

*To whom correspondence should be addressed. E-mail: Glenn.summerhayes@otago.ac.nz

Reactivity of the Gold/Water Interface During Selective Oxidation Catalysis

Bhushan N. Zope *et al.*

Science **330**, 74 (2010);
DOI: 10.1126/science.1195055